TITLE:

Prewetting couples membrane and protein phase transitions to greatly enhance coexistence in models and cells.

Yousef Bagheri[1], Mason Rouches[2], Benjamin Machta[3], Sarah L. Veatch[1]*

[1] Program in Biophysics, University of Michigan, Ann Arbor, MI USA

[2] Department of Molecular Biophysics & Biochemistry, Yale University, New Haven CT USA

[3] Department of Physics, Yale University, New Haven, CT USA

*sveatch@umich.edu

ABSTRACT

Both membranes and biopolymers can individually separate into coexisting liquid phases. Here we explore biopolymer prewetting at membranes, a phase transition that emerges when these two thermodynamic systems are coupled. In reconstitution, we couple short poly-L-Lysine and poly-L-Glutamic Acid polyelectrolytes to membranes of saturated lipids, unsaturated lipids, and cholesterol, and detect coexisting prewet and dry surface phases well outside of the region of coexistence for each individual system. Notability, polyelectrolyte prewetting is highly sensitive to membrane lipid composition, occurring at 10 fold lower polymer concentration in a membrane close to its phase transition compared to one without a phase transition. In cells, protein prewetting is achieved using an optogenetic tool that enables titration of condensing proteins and tethering to the plasma membrane inner leaflet. Here we show that protein prewetting occurs for conditions well outside those where proteins condense in the cytoplasm, and that the stability of prewet domains is sensitive to perturbations of plasma membrane composition and structure. Our work presents an example of how thermodynamic phase transitions can impact cellular structure outside their individual coexistence regions, suggesting new possible roles for phase-separation-prone systems in cell biology.

INTRODUCTION

Membranes often act as assembly sites for soluble proteins. These structures can be relatively stable, scaffolding the protein machinery needed to perform biological functions, for example at focal adhesions (1) or at specialized sites of contact between cells (2, 3). These structures can also be assembled in response to dynamic stimuli, gathering proteins that propagate signals, for example the signaling platforms that form downstream of T cell receptor activation (4, 5). In a growing number of cases, protein assembly at membranes is attributed to phase separation, driven by multivalent interactions between specific proteins (6–10). This occurs when protein combinations capable of condensing in solution are localized to membranes, often by tethering one or more components to the membrane or by including proteins that interact with specific lipids. Recent work has shown that localizing condensates to membranes can drive a range of phenomena in reconstituted systems, including inducing membrane curvature, lipid ordering, shifting phase transition temperatures, and transbilayer communication (9–17). Often overlooked is the possibility that membranes themselves can contribute to protein condensation, by tuning interactions between tethering components.

We recently developed a theory of biopolymer prewetting at membranes (18). Unlike wetting, which describes how preexisting phase separated domains spread and deform surfaces, prewetting is fundamentally a surface phenomenon that applies when phase separation is unstable in the bulk. Classical prewetting describes the condensation of liquids at solid surfaces (19, 20), and is only observed within a narrow region close to the gas-liquid transition (21). Recent theory predicts that the prewetting region expands when the surface is fluid (18, 22), in good agreement with experimental observations of protein and/or nucleic acid condensation at membranes. Our theory additionally predicts that the prewetting regime can be further expanded in the presence of membrane-mediated interactions between tethers, for example those that arise close to a membrane phase transition. Since mammalian cell plasma membranes have compositions tuned to near phase separation (23), prewetting could provide a sensitive means to organize proteins at the cell surface.

The goal of the current study is to experimentally probe these concepts in controlled reconstituted and cellular systems. Beyond demonstrating that prewet protein domains are highly sensitive to membrane properties, we show that the same forces that eventually lead to protein condensation impact structure even under conditions far from phase separation in the bulk. It is possible that the propensity of some proteins to form condensates in isolation or with overexpression could indicate their involvement in driving other thermodynamic transitions within cells.

RESULTS

Prewetting of polyelectrolyte solutions on a fluid lipid bilayer

We first explore a reconstituted system, utilizing a simplified model consisting of short poly-L-lysine (pLys) and poly-L-glutamic acid (pGlu) polyelectrolytes coupled to a supported planar membrane. pGlu and pLys mixtures are a well characterized system that undergoes complex coacervation (24). Figure 1A is a schematic representation of our experimental approach. We mix soluble pLys and pGlu polyelectrolytes in solution at an equal weight ratio in the presence of phosphate buffer (pH=7.4) and NaCl to tune the magnitude of electrostatic interactions. In the absence of a membrane, these mixtures separate into polymer condensed and dilute liquid phases over a range of polymer and NaCl concentrations (24). We also include a fluid membrane, in this case made up of a single unsaturated lipid (DOPC) along with a small fraction (4 mole%) of a reactive DOPE-DBCO lipid to facilitate covalent conjugation of an azide conjugated pLys through click chemistry (25). pLys-conjugated lipid tethers (DOPE-pLys) couple soluble polyelectrolytes to the membrane. Bilayer membranes are glass supported multilayers assembled by hydrating spin-coated lipid films to reduce the impact of the substrate (26).

By varying the concentration of soluble pLys and pGlu polymers we access three distinct regimes in the phase behavior of this coupled system (Figure 1B). At low concentration, pLys and pGlu polymers remain dispersed in solution and fluorescently labeled pLys-tethers are uniformly distributed on the (dry) membrane. At polyelectrolyte concentrations above saturation (c_{sat}), liquid condensates rich in soluble pLys and pGlu polymers are present in solution and can be visualized using a fluorescent pLys conjugate (pLys-532) and by transmitted white light. When condensates contact the bilayer, they wet the membrane, incorporating fluorescently tagged DOPE-pLys tethers (DOPE-pLys-647) at the droplet membrane interface.

At intermediate soluble pLys/pGlu concentrations, below c_{sat} but above another threshold concentration c_{prewet}, domains rich in fluorescent soluble polymers and pLys-tethers assemble at the membrane, but are not visible in transmitted light images, suggesting they represent a two dimensional (2D) surface phase. In this regime, domains also contain fewer soluble polymers than the wet condensates, indicated by a reduced intensity of pLys-532. These observations, along with the knowledge that these domains are detected under conditions where polymers are in a single phase in the bulk, lead us to conclude that they are prewet. A phase diagram characterizing regions where coexisting prewet and dry surface phases are observed as a function of soluble polyelectrolyte and NaCl concentration is shown in Figure 1C. Also shown is the analogous diagram for coexisting condensed and dilute phases in the bulk. Of note, prewet drops are detected at pLys/pGlu concentrations close to 100 fold lower than needed for polymers to separate in the bulk, over a range of NaCl concentrations. These prewet domains resemble those observed in numerous other studies that couple purified proteins or nucleic acids to membranes (7, 14, 17, 27, 27–29).

Circular prewet domains diffuse in 2D within membranes (Supplementary Movie 1) and exhibit behaviors characteristic of 2D liquid phases. Circular domains can coarsen through contact and coalescence (Figure 1D) and can themselves wet one dimensional defects within membrane preparations. Individual DOPE-pLys tethers are mobile but confined within prewet drops, as observed by tracking single molecules over time (Figure 1E) and tabulating the mean squared displacement (Figure 1F). Droplet formation is also reversible, both by acutely increasing NaCl and by washing away soluble polymers (Figure 1G,H), although the time-scales vary. We conclude that prewet domains are thermodynamic phases which are two-dimensional fluids, but that exchange of soluble polymers between prewet domains and the 3D bulk can be slow, consistent with expectations in this polyelectrolyte system (30).

Prewetting and wetting of polyelectrolytes can also be demonstrated through simulations of membranes with mobile tethers and two types of soluble polymers (Figure 1I), modifying a simulation scheme described previously (18) and as described in Methods. In simulations, tethers remain dispersed at a low soluble polymer concentration, and increasing the soluble polymer concentration produces domains consisting of clustered tethers and soluble polymers that extend one or several polymer layers above the bilayer plane but do not extend indefinitely into the bulk. Wetting occurs only at high soluble polymer concentration when condensed polymer phases are also stable in the bulk. Contours depicting the extent of polymer domains in these simulations are shown in Figure 1J.

The membrane phase transition facilitates prewetting.

We next interrogated prewetting on multicomponent membranes of DOPC, DPPC, and cholesterol (Chol) following the experimental scheme represented in Figure 2A. Planar supported membranes constructed from these lipids can demix into two coexisting phases, called liquid-ordered (Lo) and liquid-disordered (Ld) (31). In the absence of soluble polymers, Lo-Ld demixing occurs below the miscibility transition temperature and can be detected by imaging the localization of the Ld favoring probe DiO (Figure 2B). Fluorescent DOPE-pLys-647 tethers also partition into the Ld phase.

Similar to the majority DOPC membrane of Figure 1, prewet domains form with the addition of soluble pLys and pGlu to membranes containing DOPC, DPPC, Chol and pLys-tethered lipids (Figure 2C). At temperatures above the membrane phase transition, prewet domains resemble those found in the majority DOPC membrane in that they concentrate tethers and soluble polyelectrolytes. Unlike the DOPC membrane, prewet domains in ternary membranes additionally sort the fluorescent lipid analog DiO, indicating that the two surface phases have distinct compositions of bulk lipid components. Three surface phases with distinct lipid and tether concentrations can be detected at temperatures below the membrane phase transition, T_{mix}. The two phases that are poor in soluble polymers are assigned as Ld-dry and Lo-dry based on the partitioning of the Ld probe

DiO. The prewet phase is rich in DOPE-pLys tethers, soluble pLys/pGlu, and further enriched in DiO and is assigned to Ld-prewet. Analogous three phase coexistence has been reported in a related system including reconstituted proteins (9).

In our past theoretical work (18), we predicted that proximity to the membrane phase transition facilitates prewetting at membranes, and the same is observed in the modified model explored here (Supplementary Movie 5). This is experimentally validated by titrating soluble pLys/pGlu on membranes with distinct lipid compositions and at a fixed ambient temperature (37°C) above the miscibility transition temperature (T_{mix}) of the dry membrane. We investigated three membrane compositions with a fixed ratio of unsaturated (DOPE-pLys and DOPC) and DPPC lipids and varying cholesterol (Chol) concentration (Figure 2D), where in each case DOPE-pLys is held constant at 4 mole% of membrane lipids. At 37°C, dry membranes with the lowest Chol content (20%) are several degrees above their phase transition temperature, while membranes with increased Chol content (30% and 40%) are further from their transition both in temperature and in composition (Figure 4D,E). Adding soluble pLys and pGlu polymers to these membranes reveals that pre-wet domains assemble at lower polyelectrolyte concentration than required for prewetting in membranes with only DOPC and DOPE-pLys (Figure 2F). The effect is most pronounced in membranes with 20% Chol, which require 10-fold less soluble polymer for prewetting. These results are consistent with past work demonstrating that coupling phase separating proteins to membranes effectively raises T_{mix} for a single analogous lipid composition (10). Phase diagrams characterizing regions of prewet/dry coexistence as a function of soluble polyelectrolyte and NaCl concentration are shown in Figure 2G and Supplementary Figure 1.

A more exhaustive exploration of lipid ratios reveals that coupling to soluble pLys and pGlu produces coexisting surface phases over a broad range of lipid compositions (Figure 2H, and Supplementary Figure 2), extending the region of coexisting surface phases towards higher DOPC concentration. Membranes made of DPPC and DOPE-pLys are in a gel phase at 37°C, and the reduced mobility DOPE-pLys tethers acts to increase c_{prewet} close to c_{sat}, as reported previously (17) and observed in simulations with immobile tethers (Supplementary Movie 6). c_{prewet} is also elevated in membranes of DOPC, Chol, and DOPE-pLys compared to DOPC/DOPE-pLys membranes, suggesting that the non-ideal mixing at this composition gives rise to repulsion between tethers. In addition to modulating c_{prewet}, membrane composition additionally influences the adsorption of soluble pGlu to the membrane in both experiments and simulations (Supplementary Figure 3).

For the measurements of Figure 2F-H, prewetting is initiated by titrating soluble pLys/pGlu within the bulk above membranes of fixed composition and temperature. Prewetting can also be reversibly initiated by varying temperature in DOPC/DOPE-pLys/DPPC/Chol membranes, which impacts proximity to the membrane phase transition ($\Delta T = T-T_{mix}$) and also the magnitude of polymer interactions relative to the thermal energy k_BT (Figure 2I). Prewetting can also be reversibly initiated at fixed temperature and pLys/pGlu concentration by

changing membrane Chol content using methyl-β-cyclodextrin (MβCD; Figure 2J, Supplementary Movies 7,8). Extracting Chol from a 40% Chol membrane leads to the assembly of prewet domains, while loading Chol into a 20% Chol membrane leads to melting of prewet domains. This further demonstrates that polyelectrolyte prewetting is sensitive to membrane lipid composition, even when conditions that directly impact polymer interactions are maintained.

Prewetting at the plasma membrane is sensitive to perturbations of membrane composition and structure.

The same prewetting behaviors detected in the model system can be reconstituted within cells using existing optogenetic tools (32). For these measurements, we use a 3 component modular system consisting of a Cry2-motif conjugated to an anti-GFP nanobody (Cry2-αGFP), a soluble CIB1 protein conjugated to a multimeric protein (CIB1-MP), and a GFP anchored to the plasma membrane through the palmitoylated and myristoylated membrane binding domain of Lyn kinase (PM-GFP). Each protein component is conjugated to a distinguishable fluorescent tag. Upon exposure to blue light, Cry2-αGFP undergoes a conformational change that enables binding to CIB1-PM and other activated Cry2 molecules, as represented schematically in Figure 3A.

When transiently co-expressed in U2OS cells, PM-GFP uniformly labels the plasma membrane, Cry2-αGFP labels the membrane but is also abundant in the cytoplasm, and CIB1-MP is fully cytoplasmic (Supplementary Figure S4). Upon exposure to blue light, Cry2-αGFP, CIB1-MP, and PM-GFP co-assemble into puncta at the plasma membrane (Figure 3B). Imaging only Cry2-αGFP in live cells reveals that puncta are mobile and coarsen over time into circular domains through coalescence (Figure 3C and Supplementary Movie 9), resembling the phase separated prewet domains observed in fully reconstituted system of Figures 1-2. In the absence of blue illumination, puncta dissociate over tens of minutes at room temperature as Cry2 relaxes into its low-affinity state. Cytoplasmic droplets emerge in cells exposed to high levels of blue light or when the membrane targeted PM-GFP is replaced with a soluble GFP abundant in the cytoplasm. Taken together, these observations suggest that plasma membrane puncta assembled with short light exposures are a surface phase, analogous to the prewet phases observed in reconstitution. Cytoplasmic puncta that are either associated with the membrane (wet) or free-floating in the cytoplasm (dry) are distinguished from prewet puncta in that they are not exclusively imaged at the cell surface (Supplementary Figure S5).

We next quantified the stability of membrane bound and cytoplasmic domains by systematically varying exposure to blue light at room temperature (22°C), effectively titrating the concentration of binding competent Cry2α-GFP. Transient transfection results in a broad distribution of expression levels across cells and we quantify the fraction of cells containing Cry2α-GFP/CIB1-MP puncta within a population of imaged cells (>100 per condition) as described in Methods and Supplementary Figure S6. Results are summarized in the phase

diagram of Figure 3D, which shows that much shorter light exposures are required to form Cry2-αGFP/CIB1-MP puncta in cells expressing plasma membrane tethered PM-GFP as compared to cells expressing cytoplasmic GFP. This is in agreement with past findings with these constructs (33), and also analogous to the phase diagram of Figure 1C. This further supports the conclusion that membrane bound puncta are a prewet phase, in that they assemble under conditions where condensation into 3D phases does not occur in the bulk.

Mammalian cell plasma membranes are in a single phase but are tuned near a membrane miscibility transition (23, 34). Similar to prewet polyelectrolyte domains on model membranes, we sought to investigate if perturbations of plasma membrane phase behavior also alter the stability of plasma membrane localized Cry2-αGFP/CIB1-MP puncta in U2OS cells (Figure 3E). We first varied the ambient temperature of cells during light exposure and chemical fixation. At 4°C, puncta assembled with lower light doses and more cells contained puncta at high light doses, while more light was required to observe puncta in cells prepared at 37°C.

In a related measurement in live cells, Cry2-αGFP remains uniformly distributed in some cells exposed to a low dose of blue light at 37°C, but condenses into puncta following a temperature quench to 15°C (Supplemental Movie 10). Changes in ambient temperature alter proximity to the membrane phase transition, but also impact Cry2 deactivation kinetics and the relative magnitude of Cry2/Cry2 and Cry2/CIB1-MP interactions compared to the thermal energy k_BT. Likely because of this, we also detect more cells containing puncta at 4°C at intermediate light exposures in samples expressing Cry2-αGFP, CIB1-MP, and soluble GFP.

The specific impact of the membrane is better isolated using chemical perturbations of the membrane transition at fixed ambient temperature. To accomplish this, we use two n-alcohols shown previously to modulate transition temperatures in isolated giant plasma membrane vesicles (GPMVs) and alter the contrast of membrane domains in live B cell membranes (34, 35). Similar to lowering ambient temperature, cells pre-treated with 6 μM hexadecanol contained puncta at lower light doses and a larger fraction of cells contained puncta with higher light doses. This treatment raises membrane T_{mix}, reducing ΔT. In contrast, cells pre-treated with 300 μM octanol required longer light exposure to assemble puncta, resembling the trends observed in cells prepared at elevated ambient temperature. The melting of domains and desorption of Cry2-αGFP from the plasma membrane can also be detected in live cells after acute treatment with 300 μM octanol at fixed ambient temperature (Supplemental Movie 11 and Supplementary Figure S7). Unlike changing ambient temperature, octanol and hexadecanol treatments do not significantly impact the assembly of cytoplasmic puncta over a wide range of light exposures. This supports the conclusion that n-alcohol treatment alters the stability of Cry2/CIB1-MP puncta via its impact on membrane properties, likely through their effect on

T_{mix}. This is analogous to the results of Figure 2 showing that the stability of pre-wet domains can be enhanced by coupling to membranes close to their miscibility transition.

We next explored two additional perturbations expected to exert effects through changes in membrane properties without directly altering the magnitude of protein interactions (Figure 3F). The first involved perturbing plasma membrane Chol, where we found that supplementing plasma membrane Chol with MβCD-Chol stabilized Cry2/CIB1-MP puncta and depleting Chol with MβCD destabilized Cry2/CIB1-MP puncta in both chemically fixed and live cells (Supplementary movies 12,13). MβCD treatment can alter the concentration or localization of membrane components besides plasma membrane Chol (36, 37), and it is possible that some of these off-target effects contribute to this observation. We do not expect MβCD to directly impact Cry2/Cry2 or Cry2/CIB1-MP interactions, and MβCD treatment does not impact the light sensitivity of Cry2-αGFP/CIB1-MP puncta assembled in the presence of soluble GFP (Supplementary Figure S8). As a final perturbation, we treated cells with the calcium ionophore A23187. Elevated cytoplasmic Ca^{2+} activates the plasma membrane localized scramblase TMEM16, relaxing some plasma membrane leaflet asymmetry (37, 38) as detected through the binding of Annexin V on the extracellular leaf (Supplementary Figure S9). Cells pretreated with A23187 exhibit greatly diminished Cry2/CIB1-MP puncta even after long light exposure, and acute A23187 treatment leads to the dissociation of domains in live cells (Supplementary Movie 14). Many processes at the plasma membrane and within the cytoplasm are activated by high cytoplasmic Ca^{2+} (39, 40), leading to many possible off-target effects. Even so, A23187 pre-treatment does not greatly impact Cry2-αGFP/CIB1-MP puncta assembled in the presence of soluble GFP, indicating that any off-target effects relevant to the destabilization of plasma membrane localized puncta affect plasma membrane structure or composition (Supplementary Figure S8).

DISCUSSION

Here we show that prewet domains are exquisitely sensitive to properties of membranes through modeling and experiments in controlled reconstituted systems and cells. In reconstitution, we coupled two systems with well characterized miscibility transitions (24, 31), and found that prewet polyelectrolyte domains formed well outside the coexistence region of either transition. Moreover, we found that the concentration of soluble polymer required to observe prewet domains, c_{prewet}, could be varied by more than an order of magnitude solely by varying membrane lipid composition. Of note, the membrane phase transition exerts its effect even when the membrane on its own would be in a single phase, and even when crossing into the 2 phase region would require large changes in temperature and/or composition. In cells, we exploited available optogenetic tools (32) to generate prewet domains at the plasma membrane inner leaflet, using light exposure as a titratable parameter to effectively tune the concentration of binding competent protein in the cytoplasm. Here too we found that the stability of prewet domains depends strongly on membrane composition and structure, probed through a range of perturbations. Some of these perturbations have well characterized impacts on the

membrane phase transition in isolated and intact plasma membranes (34, 35), supporting a role of the membrane phase transition in tuning the stability of prewet protein assemblies at the plasma membrane even though the plasma membrane is a single liquid phase. There is remarkable consistency across the models and cell measurements, supporting the view that Universal aspects of these phase transitions underlie the assembly of domains in cells.

These studies add to a large body of emerging work interrogating both the biophysical and biological roles of condensates at membranes (6–12, 15, 17, 22, 28, 41–44). In particular, this work integrates long-standing theories of membrane domains at the plasma membrane (23, 45, 46) with the more recently appreciated concept of protein-driven condensation. In these older theories, lipid-interactions alone were thought to be sufficient to confine membrane proteins to functional signaling platforms (45, 47). More modern views of signal propagation at membranes posit instead that signaling platforms assemble exclusively from multivalent protein interactions (48). The current work suggests that cells likely exploit both miscibility transitions in the assembly of these plasma membrane structures.

Prewet domains arising from coupled biopolymer and membrane phase transitions have properties not accessible in each individual system. Proteins and nucleic acids can fold into complex structures that encode specificity not accessible to lipids, and their interactions can be regulated through a range of post-translational modifications. These properties allow condensates of proteins and/or nucleic acids to gather components required to perform specific biological functions when needed by the cell. Lipids are small molecules that generally lack specificity, but as seen in the current study, emergent properties that arise by tuning close the membrane miscibility transition can dramatically enhance sensitivity, meaning that many fewer cytosolic proteins are required for assembly. Moreover, tuning membrane properties provides a means to control the stability of diverse domains prewet at the same membrane.

More broadly, we propose that prewetting and related phenomena represent an unexplored avenue into the functional roles of protein and nucleic acid condensates in cells. While most existing work has focused on the presence and properties of phase separated domains themselves, our work suggests that condensates can structure cells even well outside of phase coexistence, through interactions with surfaces or other structures capable of enhancing condensation. In this work we focused on coupling protein condensation to the miscibility transition within membranes, but in principle a generalized prewetting phenomena could apply to other types of thermodynamic transitions, for example those involving shape transitions at membranes (14), or even polymer collapse (49). Condensates interact strongly with a variety of surfaces (50–53), and it is possible that a large fraction of condensation phenomena is driven by the thermodynamics of an underlying surface.

MATERIALS AND METHODS

Materials. All chemicals were purchased from suppliers and directly used without any further purification. All lipids including 1,2-dioleoyl-sn-glycero-3-phosphocholine (DOPC), 1,2-dipalmitoyl-sn-glycero-3-phosphocholine (DPPC), 1,2-dioleoyl-sn-glycero-3- phosphoethanolamine-N-dibenzocyclooctyl (18:1 DBCO PE), and cholesterol (Chol) were purchased from Avanti Polar Lipids (Alabaster, AL USA). MβCD (CAS#128,446-36-6) was purchased from TCI Chemicals (Portland, OR). Poly (l-glutamic acid sodium salt), CAS#26247-70-0 (MW=7500Da), Poly(l-lysine hydrobromide), CAS#25988-63-0 (MW=6300Da) and Poly(l-lysine hydrobromide) azide, CAS# 25988-63-0 (MW=6300Da) was purchased from Alamanda polymers (Huntsville, AL, USA). Fluorescent lipid analog 3,3'-Dioctadecyloxacarbocyanine Perchlorate (DiO-C18) (Cat#: D3898), Alexa Fluor 532 NHS Ester (Succinimidyl Ester) (Cat# A20101MP) and Ionophore A23187 (Cat# J63020.MA) were purchased from Thermo Fisher Scientific (Waltham, MA, USA). CF 647 succinimidyl ester (Cat# SCJ4600048) was purchased from millipore sigma. SNAP-Cell 647-SiR (Cat#S9102S) was purchased from New England Biolabs. Unless otherwise indicated, remaining reagents were purchased from MilliporeSigma (Burlington, MA, USA)

Fluorescent labeling of polymers. pLys-N3, pGlu, and pLys (1eq) were modified with a fluorophore containing an NHS ester (5eq) in PBS buffer (pH= 7.4) at room temperature for 1 hour. Unreacted probe was removed by passing the reaction mixture through Amicron Ultra column with 3k cutoff size. pLys-N3 was coupled to CF 646 and pLys and pGlu were each conjugated to Alexa 532.

Preparation of supported lipid bilayers. Lipid bilayers were prepared by spin-coating following previous protocols (13). Briefly, the specified lipid solutions plus an additional 0.2 mole% DiO were measured from concentrated stock solutions in chloroform and dried under vacuum. The dried lipid film was resuspended in 96% chloroform and 4% methanol to a final lipid concentration of 1.5mg/ml, then 40ul of this solution was spin coated on a clean glass substrate for 30 seconds at 3000 rpm. Glass substrates were either conventional coverslips (Thermo Fisher scientific Cat# 174969) or smart glass substrates (18x18x0.17 mm³, Interherence GmbH, Erlangen, Germany) for temperature controlled measurements. In both cases, substrates were plasma cleaned (Harrick plasma PDC-32G) prior to spin-coating. The glass supported lipid film was then dried under vacuum for 30 min to remove residual solvent. The dried lipid layer was rehydrated with 200µl phosphate buffered saline (PBS), prior to labeling with 2µg/ml CF647-pLys-N3 using a copper free click reaction with 18:1 DBCO PE at 37°C temperature for 30 minutes. Unreacted polymer was removed by exchanging the buffer above the membrane three times with PBS or PBS supplemented with NaCl. Prior to additional experimentation, DiO (blue excitation) and DOPE-pLys-647 (red excitation) were imaged to verify pLys conjugation and the presence of a contiguous bilayer.

Preparation of polyelectrolyte solutions. Unmodified pLys and pGlu were separately diluted from concentrated stocks into solutions containing phosphate buffer (pH 7.4) and the desired NaCl concentration,

then mixed in a 1:1 (w/w) ratio immediately prior to observation, typically within the imaging chamber. In some measurements, 10% of the respective polymer was replaced by its fluorescent analog (pLys-532 or pGlu-532) to enable imaging of soluble components.

Preparation of MβCD-chol: MβCD (5 mg/ml) was dissolved in a PBS buffer and degassed for 30 minutes under vacuum and stored under Argon to prevent oxidation. Saturated MβCD/Chol solutions were prepared by first wetting 18 mg of powdered cholesterol with 200μL of methanol, drying under nitrogen, then resuspending in 5mg/ml MβCD solution (24 ml). This suspension was vortexed then sonicated (twice each for 2min) using a Branson bath Ultrasonifier (MODEL S450A, Process Equipment & Supply Inc, North Olmsted OH). This suspension was stored at room temperature with continuous rotation and was typically used at least 12 h after preparation. Immediately prior to an experiment, the equilibrated solution was filtered through stacked 0.2 and 0.1μm Millex-VV Syringe Filter Units to remove cholesterol crystals.

Polymer condensation in solution and at supported membranes. Phase boundaries were determined by titrating soluble polymers at constant NaCl concentration at constant temperature while monitoring the distribution of fluorescent signals by microscopy. Typically, measurements were performed within a temperature controlled imaging chamber using a VAHEAT stage (Interherence) with PDMS (polydimethylsiloxane) reservoir held at 37°C. Polyelectrolyte concentration was titrated by adding small volumes of concentrated stocks to achieve the desired final concentration in solution. Systems exhibiting puncta in the majority of fields of view were assigned to contain coexisting phases. In some experiments, NaCl concentration was changed acutely by adding a small volume of a concentrated solution at the microscope stage. Cholesterol was added or removed from supported membranes by adding 150μl of either MβCD or MβCD-Chol with added polymers to 150μl of polymer solutions on the microscope stage. In absorption measurements, bright puncta visible in pGlu-532 images were segmented using a threshold whose level was set at 3 times the standard deviation of the first level wavelet of individual images. The total area fraction of segments (not shown) depended on details of how the binarization was accomplished, but the average intensity of segmented regions was robust to segmentation parameters.

Preparation of U2OS cells. Human Bone Osteosarcoma Epithelial Cells (U2OS) (ATCC HTP-96) were obtained from Phyllis Hanson (University of Michigan, Ann Arbor MI.) Cells were transiently transfected with plasmid-DNA encoding pCMV-CIB1-mRFP1-MP (addgene #58367)(32), pCMV-SNAP-CRY2-VHH(GFP) (addgene #58370)(32) and either PM-GFP (a gift from Barbara Baird and David Holowka, Cornell University, Ithaca, NY) (54) or soluble eGFP (Lonza) using Nucleofector electroporation (Lonza, Basel, Switzerland) with electroporation program CM-104. Generally, 500K cells were transfected with 1.5μg of total plasmid DNA and incubated overnight in glass-bottom culture dishes (P35G-1.5-10) (Mattek; Massachusetts, USA). For measurements involving multiple conditions that are compared directly, transfected cells are pooled prior to

plating into dishes. Prior to an experiment, cells were labeled with the SNAP ligand SNAP-Cell 647-SiR following the manufacturer protocol. For fixed cell measurements, cells in imaging buffer (119 mM NaCl, 5 mM KCl, 25 mM HEPES buffer, 2 mM CaCl2, 2 mM MgCl2, 6 g/liter glucose, pH to 7.4) were exposed to controlled doses of blue light on a invitrogen gel imager (Safe Imager™ 2.0, Cat# G6600) prior to chemical fixation in 2% formaldehyde with 0.15% Glutaraldehyde for 10 min at room temperature. The fixative was then quenched with 3% Bovine serum albumin and imaged in the imaging buffer. In live cell experiments, cells in the imaging buffer were exposed to blue light through the objective using the epi-fluorescence light-source immediately prior to imaging.

For fixed cell measurements involving temperature perturbations, the light box was placed inside an incubator (37°C) or a cold room (4°C). Cells were equilibrated at the treatment temperature for 15 min prior to light exposure and fixation. For fixed cells pre-treated with n-alcohols, 5uL of concentrated DMSO stocks of either 1-octanol (120mM), 1-hexadecanol (6mM), or DMSO alone were diluted directly into 2ml of imaging buffer. Cells were incubated at room temperature for 5 min before light exposure and chemical fixation. In the case of MβCD treatment, cells were incubated with 10 mM of MβCD at room temperature for 10 minutes prior to the light exposure and fixation. For MβCD/Chol treatment,saturated MβCD/Chol mixture was directly added to the cells without dilution and incubated at room temperature for 10 minutes followed by desired light exposure and fixation. For fixed cell measurements involving ionophore A23187 treatment, cells were incubated with 10μM of ionophore in the imaging buffer for 3 minutes prior to light exposure and chemical fixation. In separate measurements, PS exposure was monitored by Annexin V (Thermofisher, Cat#A23204) binding.

In live cell measurements with acute treatments, cells were exposed to light prior to imaging and treatment. Perturbations were added to dishes after light exposure at room temperature as described for fixed cell measurements, with the exception of cholesterol perturbations in which the described solution was diluted 1:1. For temperature manipulation in live cell measurements, cells were plated on smart substrate and imaged as described for supported bilayer measurements with temperature control. Temperature was lowered below ambient temperature using Cold Gun System (Exair, Cat# 5215) mounted on the microscope.

Quantifying cells containing puncta in fixed cell measurements. Multiple 82μm by 82μm fields of view (typically 20) within dishes were imaged in 3 colors to separately detect Cry2 (red excitation), CIB1-MP (green excitation), and GFP (blue excitation). Fields of view were collected randomly across the dish and typically contained 1-10 cells per field. After collecting an entire dataset spanning different treatments and light exposures, fields of view were randomized and cells within images were manually annotated by a separate individual blinded to the experimental conditions. Cells contained a broad distribution of expression levels and all cells expressing detectable levels of any labeled protein were annotated. Cells were determined to contain puncta if both the Cry2 and CIB1 channels exhibited multiple colocalized clusters.

Fluorescence imaging. Planar supported bilayers were imaged using an Olympus IX83-XDC inverted microscope with 100X UAPO TIRF objective (NA = 1.49), and active Z-drift correction (ZDC) (Olympus America). Fluorescence excitation was performed using LED lamp and fluorescence emission was detected on an EMCCD camera (Ultra 897, Andor). Different color channels were isolated using appropriate filter cubes (Chroma,Bellows Falls, VT USA). Single pLys-647 polymers were detected through total internal reflection illumination using a 647nm laser (OBIS 647, 120mW, Coherent, Santa Clara, CA) and single molecules were localized and tracked as described previously (34).

Diffraction limited images of chemically fixed and live cells were acquired on the IX83 microscope described above, or on a similarly equipped Olympus IX81 microscope. Confocal images of chemically fixed cells were acquired using ZEIS LSM 980 with Airyscan 2 Confocal microscope with plan-apochromat 63x/1.40 oil DIC M27 objective and GaAsP-PMT detector.

Monte-Carlo Simulations

Simulation Framework — We performed Monte-Carlo simulations on a 3-Dimensional DxLxL lattice. We impose periodic boundary conditions on the two lateral *L* dimensions, and free boundary conditions at the *D=0* and *D=L boundaries* of the third z dimension. Our bulk system consists of two soluble polymers whose interactions we describe by a simple Hamiltonian:

$$H_{bulk} = -J_{bulk}\sum_i \sigma_i^1\sigma_i^2 - J_{nn}\sum_{i,j\,\epsilon\,nn}\sigma_i\sigma_j - \frac{\mu_{bulk}}{n_{bulk}}\sum_i(\sigma_i^1 + \sigma_i^2)$$

Here J_{bulk} resembles the interaction strength between pLys and pGlu polymers in our experiments (tuned by salt concentration), J_m is a non-specific interaction, μ_{bulk} is the chemical potential per bulk molecule, which sets the concentration, and n_{bulk} = 10 is the number of monomers per bulk molecule. The superscripts 1 and 2 denote the two different polymer species that interact with each other, but self avoid.

We model a lipid membrane on the *z=0* boundary of our simulations. We add interactions with the membrane through a 'tethered' polymer component held at fixed concentration and restricted to diffusion in 2D in the membrane plane. These tethers resemble the 2nd bulk polymer species above, except the length of tethers is n_{tether} = 5 monomers. The interactions between the tethered polymers and the bulk are captured by the Hamiltonian:

$$H_{tether} = -J_{buk}\sum_i \sigma_i^1\sigma_i^{tether}$$

In simulations where we model a multicomponent membrane, we additionally include an ising model at the z=*0* boundary of the simulation box. The energetics of the Ising model are described by the Hamiltonian:

$$H_{mem} = -J_{mem} \sum_{i,j \in nn} s_i s_j$$

where s_i and s_j are spins at lattice positions i and j, and the sum runs over all nearest-neighbors. Here J_{mem} sets the strength of interactions in the Ising model, and we fix the magnetization and thus have no magnetic field term.

Simulation Procedure We sample configurations of these simulations with a Monte-Carlo procedure. Bulk molecules are free to move in the simulation box, and their configurations are updated with local `kink' and `reptation' moves. These moves are accepted with the Metropolis probability $p_{accept} = max(e^{\beta H}, 1)$. We also propose translations of clusters of bulk molecules. We only accept these cluster moves if no bonds are formed or broken during the move, following detailed balance. We exchange bulk molecules with a particle reservoir, whose acceptance probability is set by the Hamiltonian above.

We update tether molecules with translations in the plane of the membrane, which are again accepted with a Metropolis probability. In simulations modeling membranes with immobile tethers we do not propose any tether moves. In simulations with the Ising membrane, the tether can only move on s_i= -1 membrane spins, to mimic the coupling to a specific membrane phase. Likewise, we reject any ising spin-exchanges that attempt to flip a spin on the same position as a tether. We simulate the ising model with conserved-spin, local Kawasaki dynamics where spin-exchanges are only proposed among nearest-neighbors. Each Monte-Carlo step of our simulation proposes updates for every particle and spin, and a number of particle exchanges with the reservoir. We ran simulations up to ~10^8 Monte-Carlo steps to ensure equilibration.

Adsorption Isotherms To calculate the adsorption in our simulations, we first identify whether a prewet phase is present. We then identify *dense-phase* domains as lattice points where the time-averaged density of tether and bulk molecules is greater than or equal to a threshold value of 1. After identifying these regions we average the density in the dense phase over the two lateral dimensions at each *z* coordinate, and then sum the final density over *z.* When the average area fraction of domains is below $16/64^2$ we declare the system as *single-phase*, and average the density over all lateral coordinates before summing over *z.* For immobile tether simulations, we average these results over ten random tether configurations.

ACKNOWLEDGEMENTS

We thank Guoming Gao for assistance with some early experiments, and Andrea Stoddard for support with molecular biology and cell culture. Research was supported through grants from the NSF (1808551 to BBM and SLV) and the NIH (GM138341 to BBM and GM152150 to SLV).

CITED REFERENCES

1. Mishra, Y.G., and B. Manavathi. 2021. Focal adhesion dynamics in cellular function and disease. *Cell. Signal.* 85:110046.
2. Zihni, C., C. Mills, K. Matter, and M.S. Balda. 2016. Tight junctions: from simple barriers to multifunctional molecular gates. *Nat. Rev. Mol. Cell Biol.* 17:564–580.
3. Kaizuka, T., and T. Takumi. 2018. Postsynaptic density proteins and their involvement in neurodevelopmental disorders. *J. Biochem. (Tokyo)*. 163:447–455.
4. Courtney, A.H., W.-L. Lo, and A. Weiss. 2018. TCR Signaling: Mechanisms of Initiation and Propagation. *Trends Biochem. Sci.* 43:108–123.
5. McAffee, D.B., M.K. O'Dair, J.J. Lin, S.T. Low-Nam, K.B. Wilhelm, S. Kim, S. Morita, and J.T. Groves. 2022. Discrete LAT condensates encode antigen information from single pMHC:TCR binding events. *Nat. Commun.* 13:7446.
6. Su, X., J.A. Ditlev, E. Hui, W. Xing, S. Banjade, J. Okrut, D.S. King, J. Taunton, M.K. Rosen, and R.D. Vale. 2016. Phase separation of signaling molecules promotes T cell receptor signal transduction. *Science*. 352:595–599.
7. Zeng, M., X. Chen, D. Guan, J. Xu, H. Wu, P. Tong, and M. Zhang. 2018. Reconstituted Postsynaptic Density as a Molecular Platform for Understanding Synapse Formation and Plasticity. *Cell*. 174:1172-1187.e16.
8. Case, L.B., M. De Pasquale, L. Henry, and M.K. Rosen. 2022. Synergistic phase separation of two pathways promotes integrin clustering and nascent adhesion formation. *eLife*. 11:e72588.
9. Wang, H.-Y., S.H. Chan, S. Dey, I. Castello-Serrano, M.K. Rosen, J.A. Ditlev, K.R. Levental, and I. Levental. 2023. Coupling of protein condensates to ordered lipid domains determines functional membrane organization. *Sci. Adv.* 9:eadf6205.
10. Chung, J.K., W.Y.C. Huang, C.B. Carbone, L.M. Nocka, A.N. Parikh, R.D. Vale, and J.T. Groves. 2021. Coupled membrane lipid miscibility and phosphotyrosine-driven protein condensation phase transitions. *Biophys. J.* 120:1257–1265.
11. Mangiarotti, A., N. Chen, Z. Zhao, R. Lipowsky, and R. Dimova. 2023. Wetting and complex remodeling of membranes by biomolecular condensates. *Nat. Commun.* 14:2809.
12. Mangiarotti, A., M. Siri, N.W. Tam, Z. Zhao, L. Malacrida, and R. Dimova. 2023. Biomolecular condensates modulate membrane lipid packing and hydration. *Nat. Commun.* 14:6081.
13. Zeno, W.F., K.E. Johnson, D.Y. Sasaki, S.H. Risbud, and M.L. Longo. 2016. Dynamics of Crowding-Induced Mixing in Phase Separated Lipid Bilayers. *J. Phys. Chem. B*. 120:11180–11190.
14. Yuan, F., H. Alimohamadi, B. Bakka, A.N. Trementozzi, K.J. Day, N.L. Fawzi, P. Rangamani, and J.C. Stachowiak. 2021. Membrane bending by protein phase separation. *Proc. Natl. Acad. Sci.* 118:e2017435118.
15. Mondal, S., K. Narayan, S. Botterbusch, I. Powers, J. Zheng, H.P. James, R. Jin, and T. Baumgart. 2022. Multivalent interactions between molecular components involved in fast endophilin mediated endocytosis drive protein phase separation. *Nat. Commun.* 13:5017.
16. Lee, Y., S. Park, F. Yuan, C.C. Hayden, L. Wang, E.M. Lafer, S.Q. Choi, and J.C. Stachowiak. 2023. Transmembrane coupling of liquid-like protein condensates. *Nat. Commun.* 14:8015.
17. Snead, W.T., A.P. Jalihal, T.M. Gerbich, I. Seim, Z. Hu, and A.S. Gladfelter. 2022. Membrane surfaces regulate assembly of ribonucleoprotein condensates. *Nat. Cell Biol.* 24:461–470.
18. Rouches, M., S.L. Veatch, and B.B. Machta. 2021. Surface densities prewet a near-critical membrane. *Proc. Natl. Acad. Sci.* 118:e2103401118.
19. Nakanishi, H., and M.E. Fisher. 1982. Multicriticality of Wetting, Prewetting, and Surface Transitions. *Phys. Rev. Lett.* 49:1565–1568.
20. Cahn, J.W. 1977. Critical point wetting. *J. Chem. Phys.* 66:3667–3672.
21. Schmidt, J.W., and M.R. Moldover. 1986. A search for the prewetting line. *J. Chem. Phys.* 84:4563–4568.
22. Zhao, X., G. Bartolucci, A. Honigmann, F. Jülicher, and C.A. Weber. 2021. Thermodynamics of wetting, prewetting and surface phase transitions with surface binding. *New J. Phys.* 23:123003.
23. Veatch, S.L., N. Rogers, A. Decker, and S.A. Shelby. 2023. The plasma membrane as an adaptable fluid mosaic. *Biochim. Biophys. Acta BBA - Biomembr.* 1865:184114.

24. Priftis, D., and M. Tirrell. 2012. Phase behaviour and complex coacervation of aqueous polypeptide solutions. *Soft Matter*. 8:9396–9405.
25. Baskin, J.M., J.A. Prescher, S.T. Laughlin, N.J. Agard, P.V. Chang, I.A. Miller, A. Lo, J.A. Codelli, and C.R. Bertozzi. 2007. Copper-free click chemistry for dynamic *in vivo* imaging. *Proc. Natl. Acad. Sci.* 104:16793–16797.
26. Weakly, H.M.J., and S.L. Keller. 2024. Coupling liquid phases in 3D condensates and 2D membranes: Successes, challenges, and tools. *Biophys. J.* 123:1329–1341.
27. Banjade, S., and M.K. Rosen. 2014. Phase transitions of multivalent proteins can promote clustering of membrane receptors. *eLife*. 3:e04123.
28. Lin, C.-W., L.M. Nocka, B.L. Stinger, J.B. DeGrandchamp, L.J.N. Lew, S. Alvarez, H.T. Phan, Y. Kondo, J. Kuriyan, and J.T. Groves. 2022. A two-component protein condensate of the EGFR cytoplasmic tail and Grb2 regulates Ras activation by SOS at the membrane. *Proc. Natl. Acad. Sci.* 119:e2122531119.
29. Case, L.B., X. Zhang, J.A. Ditlev, and M.K. Rosen. 2019. Stoichiometry controls activity of phase-separated clusters of actin signaling proteins. *Science*. 363:1093–1097.
30. Ronceray, P., Y. Zhang, X. Liu, and N.S. Wingreen. 2022. Stoichiometry Controls the Dynamics of Liquid Condensates of Associative Proteins. *Phys. Rev. Lett.* 128:038102.
31. Veatch, S.L., and S.L. Keller. 2003. Separation of Liquid Phases in Giant Vesicles of Ternary Mixtures of Phospholipids and Cholesterol. *Biophys. J.* 85:3074–3083.
32. Lee, S., H. Park, T. Kyung, N.Y. Kim, S. Kim, J. Kim, and W.D. Heo. 2014. Reversible protein inactivation by optogenetic trapping in cells. *Nat. Methods*. 11:633–636.
33. Che, D.L., L. Duan, K. Zhang, and B. Cui. 2015. The Dual Characteristics of Light-Induced Cryptochrome 2, Homo-oligomerization and Heterodimerization, for Optogenetic Manipulation in Mammalian Cells. *ACS Synth. Biol.* 4:1124–1135.
34. Shelby, S.A., I. Castello-Serrano, K.C. Wisser, I. Levental, and S.L. Veatch. 2023. Membrane phase separation drives responsive assembly of receptor signaling domains. *Nat. Chem. Biol.* 19:750–758.
35. Machta, B.B., E. Gray, M. Nouri, N.L.C. McCarthy, E.M. Gray, A.L. Miller, N.J. Brooks, and S.L. Veatch. 2016. Conditions that Stabilize Membrane Domains Also Antagonize n-Alcohol Anesthesia. *Biophys. J.* 111:537–545.
36. Ottico, E., A. Prinetti, S. Prioni, C. Giannotta, L. Basso, V. Chigorno, and S. Sonnino. 2003. Dynamics of membrane lipid domains in neuronal cells differentiated in culture1. *J. Lipid Res.* 44:2142–2151.
37. Doktorova, M., J.L. Symons, X. Zhang, H.-Y. Wang, J. Schlegel, J.H. Lorent, F.A. Heberle, E. Sezgin, E. Lyman, K.R. Levental, and I. Levental. 2023. Cell Membranes Sustain Phospholipid Imbalance Via Cholesterol Asymmetry. 2023.07.30.551157.
38. Suzuki, J., M. Umeda, P.J. Sims, and S. Nagata. 2010. Calcium-dependent phospholipid scrambling by TMEM16F. *Nature*. 468:834–838.
39. Clapham, D.E. 2007. Calcium Signaling. *Cell*. 131:1047–1058.
40. Stefan, C.J. 2020. Endoplasmic reticulum–plasma membrane contacts: Principals of phosphoinositide and calcium signaling. *Curr. Opin. Cell Biol.* 63:125–134.
41. Wiegand, T., J. Liu, A.W. Fritsch, L. Vogeley, I. LuValle-Burke, J. Geisler, A.A. Hyman, and S.W. Grill. 2024. Actin polymerization counteracts prewetting of N-WASP on supported lipid bilayers. .
42. Zhu, S., Z. Shen, X. Wu, W. Han, B. Jia, W. Lu, and M. Zhang. 2024. Demixing is a default process for biological condensates formed via phase separation. *Science*. 384:920–928.
43. Lin, C.-C., K.M. Suen, P.-A. Jeffrey, L. Wieteska, J.A. Lidster, P. Bao, A.P. Curd, A. Stainthorp, C. Seiler, H. Koss, E. Miska, Z. Ahmed, S.D. Evans, C. Molina-París, and J.E. Ladbury. 2022. Receptor tyrosine kinases regulate signal transduction through a liquid-liquid phase separated state. *Mol. Cell*. 82:1089-1106.e12.
44. Pombo-García, K., O. Adame-Arana, C. Martin-Lemaitre, F. Jülicher, and A. Honigmann. 2024. Membrane prewetting by condensates promotes tight-junction belt formation. *Nature*. 632:647–655.
45. Simons, K., and E. Ikonen. 1997. Functional rafts in cell membranes. *Nature*. 387:569–572.
46. Sezgin, E., I. Levental, S. Mayor, and C. Eggeling. 2017. The mystery of membrane organization: composition, regulation and roles of lipid rafts. *Nat. Rev. Mol. Cell Biol.* 18:361–374.
47. Simons, K., and D. Toomre. 2000. Lipid rafts and signal transduction. *Nat. Rev. Mol. Cell Biol.* 1:31–39.
48. Case, L.B., J.A. Ditlev, and M.K. Rosen. 2019. Regulation of Transmembrane Signaling by Phase Separation. *Annu. Rev. Biophys.* 48:465–494.

49. Rouches, M.N., and B.B. Machta. 2024. Polymer Collapse and Liquid-Liquid Phase-Separation are Coupled in a Generalized Prewetting Transition. .
50. Milovanovic, D., Y. Wu, X. Bian, and P. De Camilli. 2018. A liquid phase of synapsin and lipid vesicles. *Science*. 361:604–607.
51. Böddeker, T.J., K.A. Rosowski, D. Berchtold, L. Emmanouilidis, Y. Han, F.H.T. Allain, R.W. Style, L. Pelkmans, and E.R. Dufresne. 2022. Non-specific adhesive forces between filaments and membraneless organelles. *Nat. Phys.* 18:571–578.
52. Morin, J.A., S. Wittmann, S. Choubey, A. Klosin, S. Golfier, A.A. Hyman, F. Jülicher, and S.W. Grill. 2022. Sequence-dependent surface condensation of a pioneer transcription factor on DNA. *Nat. Phys.* 18:271–276.
53. Liu, S., X. Zhang, X. Yao, G. Wang, S. Huang, P. Chen, M. Tang, J. Cai, Z. Wu, Y. Zhang, R. Xu, K. Liu, K. He, Y. Wang, L. Jiang, Q.A. Wang, L. Rui, J. Liu, and Y. Liu. 2024. Mammalian IRE1α dynamically and functionally coalesces with stress granules. *Nat. Cell Biol.* 26:917–931.
54. Pyenta, P.S., D. Holowka, and B. Baird. 2001. Cross-Correlation Analysis of Inner-Leaflet-Anchored Green Fluorescent Protein Co-Redistributed with IgE Receptors and Outer Leaflet Lipid Raft Components. *Biophys. J.* 80:2120–2132.

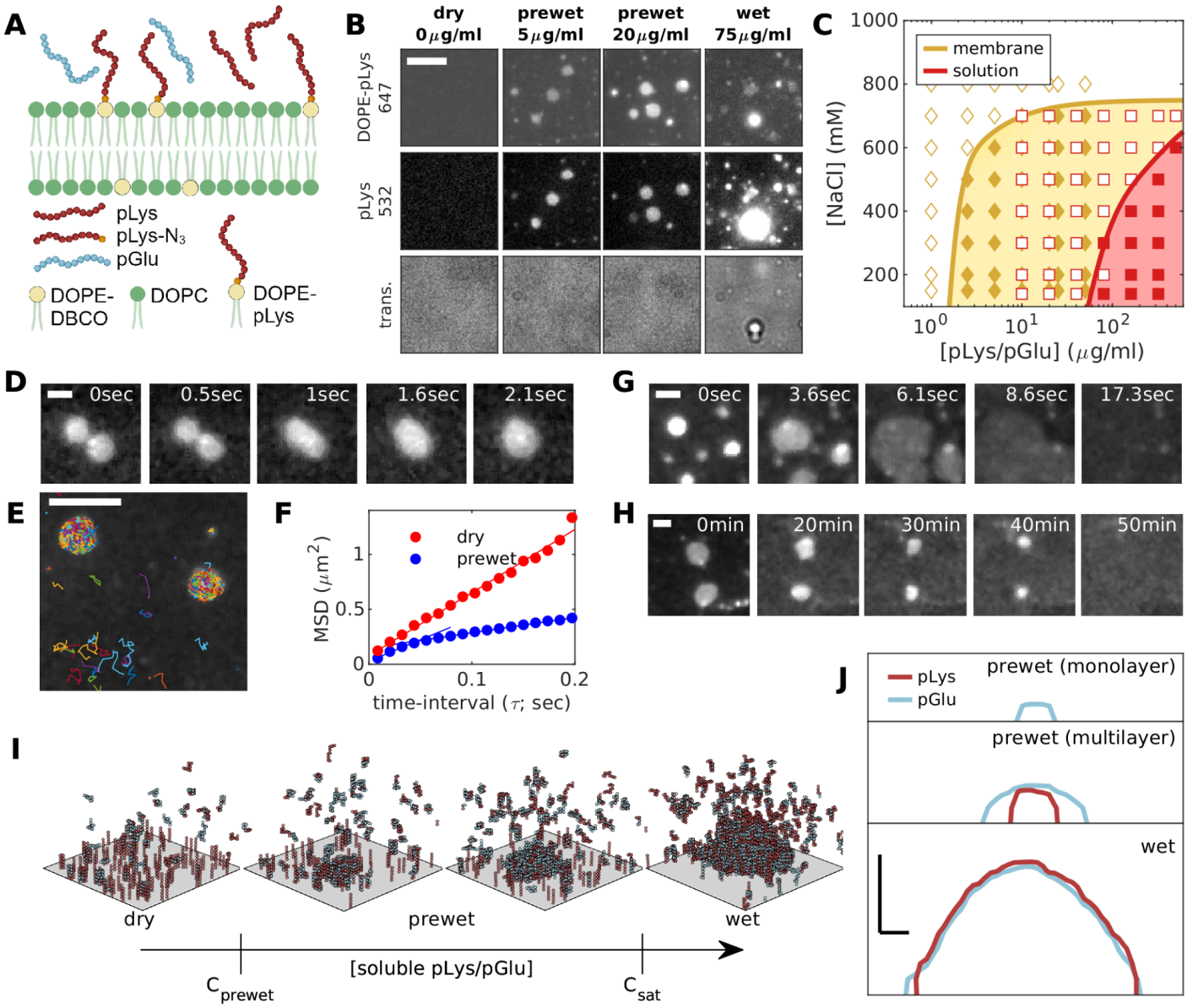

Figure 1: polyelectrolyte prewetting at simple membranes. (A) Schematic representation of the experimental system containing bulk pLys and pGlu polyelectrolytes in contact with a DOPC membrane with DOPE-pLys tethers. (B) Membranes exposed to varying concentrations of 1:1 w/w pLys/pGlu polyelectrolytes in the presence of 300mM NaCl. Prewet domains containing tethers (DOPC-pLys-647) and soluble polymer (pLys-532) are observed at intermediate polyelectrolyte concentrations (5 and 20μg/ml) while wetting is detected at high concentrations (75μg/ml). Wet but not prewet domains visible in transmitted light images. (C) Phase diagram marking polyelectrolyte and NaCl concentration where prewet (yellow) or bulk (red) domains are detected in microscopy images. (D) Prewet domains are dynamic, circular, and can coarsen via coalescence. Images are snapshots from Supplementary Movie 1. (E) Single molecule trajectories of tethers reveal they are dynamic and (F) plots of the mean squared displacement (MSD) vs time-interval for domain localized tethers are sub-linear, indicating they are confined. (G) Prewet polyelectrolyte domains dissipate when exposed to high NaCl concentration (2M) and when (H) soluble polyelectrolytes are removed from solution. Images are snapshots from Supplementary Movies 2,3. Scale bar is 5μm in B,E and 2μm in D,G, H. Panels D-H image DOPE-pLys-647. (I) Simulation snapshots of a simplified lattice model replicating essential elements of the experimental system. Movie is shown in Supplementary Movie 4. (J) Contours indicating regimes of high soluble polyelectrolyte concentration corresponding to the snapshots in I. Scale bar is 5 lattice spacings.

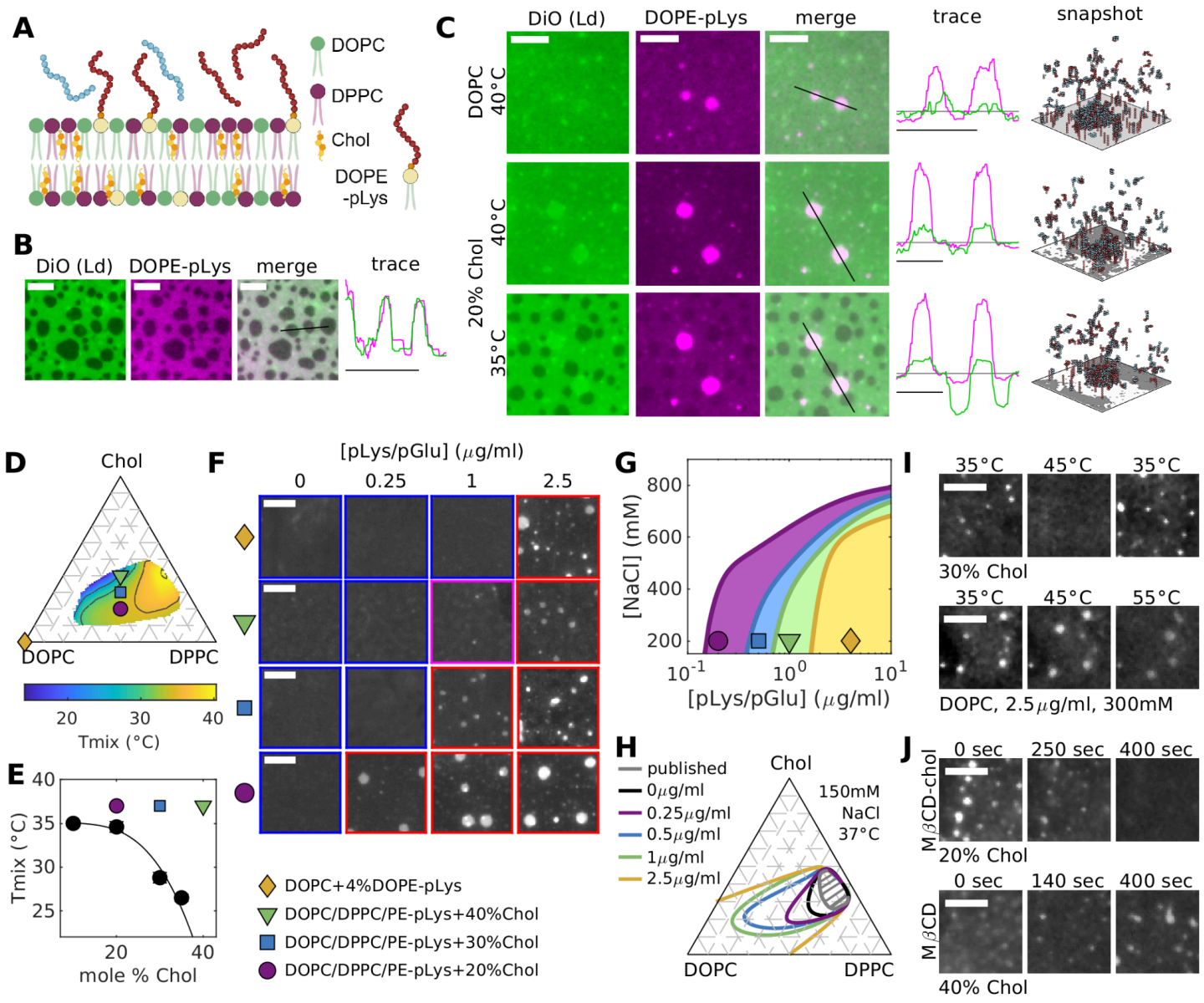

Figure 2: Proximity to the membrane phase transition enhances prewetting. (A) Schematic representation of the experimental system containing bulk pLys and pGlu in contact with membranes of DOPC, DPPC, Chol, and DOPE-pLys tethers. (B) Membranes of 36%DOPC/40%DPPC/4% DOPE-pLys/20%Chol separate into two coexisting surface phases (Lo and Ld) at 22°C. Both the lipid probe (DiO) and the tether (DOPE-pLys-647) label the Ld phase. (C) Membranes of 96%DOPC/4%DOPE-pLys (top) or 36%DOPC/40%DPPC/4% DOPE-pLys/20%Chol (middle and bottom) with 5μg/ml 1:1 w/w pLys/pGlu in the presence of 300mM NaCl. Two coexisting surface phases, prewet and dry, are detected with both membrane compositions at 40°C with tether-rich prewet domains also enriching the DiO lipid probe in the membrane with DOPC,DPPC and Chol. At 35°C, the DOPC/DPPC/Chol membrane contains 3 surface phases, Lo-dry, Ld-dry, and Ld-prewet, each with different compositions of both tether and DiO. Simulation snapshots for conditions mimicking the experimental condition are also shown. (D) Surface depicting the onset of coexisting Lo and Ld phases in membranes of DOPC, DPPC, and Chol from past work (31) along with compositions probed in this study. (E) Measured transition temperatures (black points) for compositions that incorporate 4 mol% DOPE-pLys in place of DOPC. (F) Micrographs showing DOPE-pLys-647 in the presence of the indicated 1:1 (w/w) mixtures of soluble pLys and pGlu. (G) Phase diagram for the membrane compositions from F. Individual points are shown in Supplementary Figure 1. (H) Estimated ternary phase boundary for varying soluble pLys/pGlu at constant temperature and [NaCl]. Phase diagram showing points and images are in Supplementary Figure S2. (I) Prewet domains reversibly dissipate when temperature is raised and lowered in 30% Chol membranes but not in DOPC membranes. (J) Prewet domains dissipate or form when Chol is added or removed with MBCD-Chol or MBCD respectively. Images I,J represent frames from movies supplied as Supplementary Movies 5,6. All scale bars are 5um.

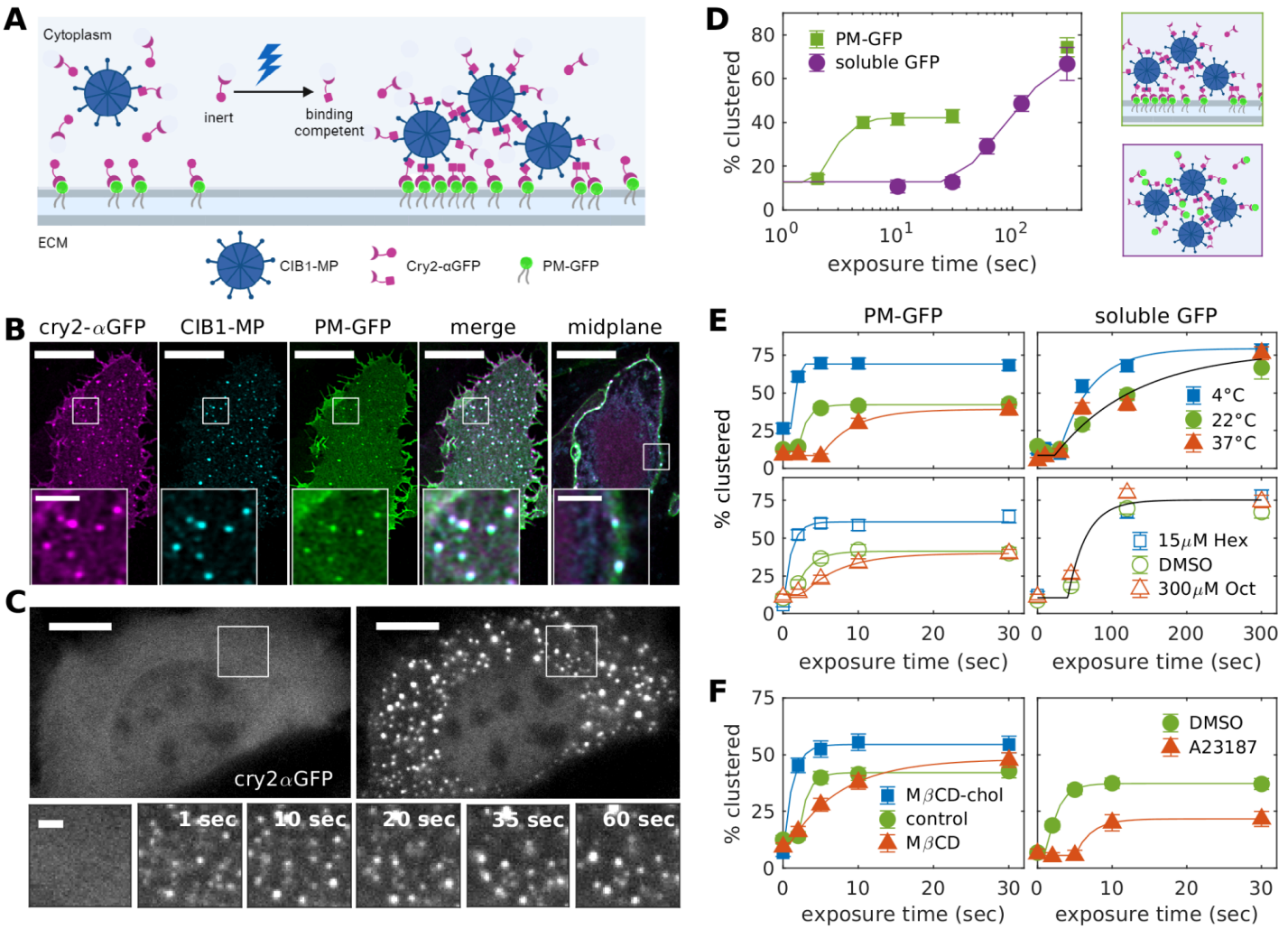

Figure 3: Prewetting at the plasma membrane is sensitive to perturbations of membrane structure and composition. (A) Schematic representation of the optogenetic system containing multivalent C1B1-MP, Cry2-αGFP, and a membrane anchored PM-GFP. Upon exposure to blue light, Cry2-αGFP can interact with itself and/or CIB1-MP. (B) Images of the 3 components co-expressed in U2OS cells chemically fixed after 5 sec of light exposure. Puncta enriched in all 3 components are present on the dorsal surface and localize to the plasma membrane in a midplane slice. (C) (Top) Live U2OS cell imaged at 37°C before (left) and after a brief exposure to blue light. (Bottom) Insets from above showing domain coarsening over time. Images are frames from Supplementary Movie 7. (D) Curves representing the percentages of cells exhibiting Cry2-αGFP/CIB1-MP puncta in fields of cells chemically fixed after the varying exposure times to blue light. Cells either co-express PM-GFP or a soluble form of GFP. Representative fields for several light exposures are shown in Supplementary Figure S6. (E) Curves representing the percentage of cells with Cry2-αGFP/CIB1-MP puncta in cells treated and chemically fixed at different ambient temperatures (top) or in the presence of n-alcohols (bottom). (F) Curves representing the percentage of cells with Cry2-αGFP/CIB1-MP puncta in cells treated and chemically fixed after Chol modulation with MβCD or MβCD-Chol (left) or in the presence of the calcium ionophore A23187 (right). Analogous curves for cells expressing soluble GFP are in Supplementary Figure S8. Scale bars are 10 μm in main images and 2 μm in insets. Movies showing the perturbations of E,F in live cells are shown in Supplementary Movies

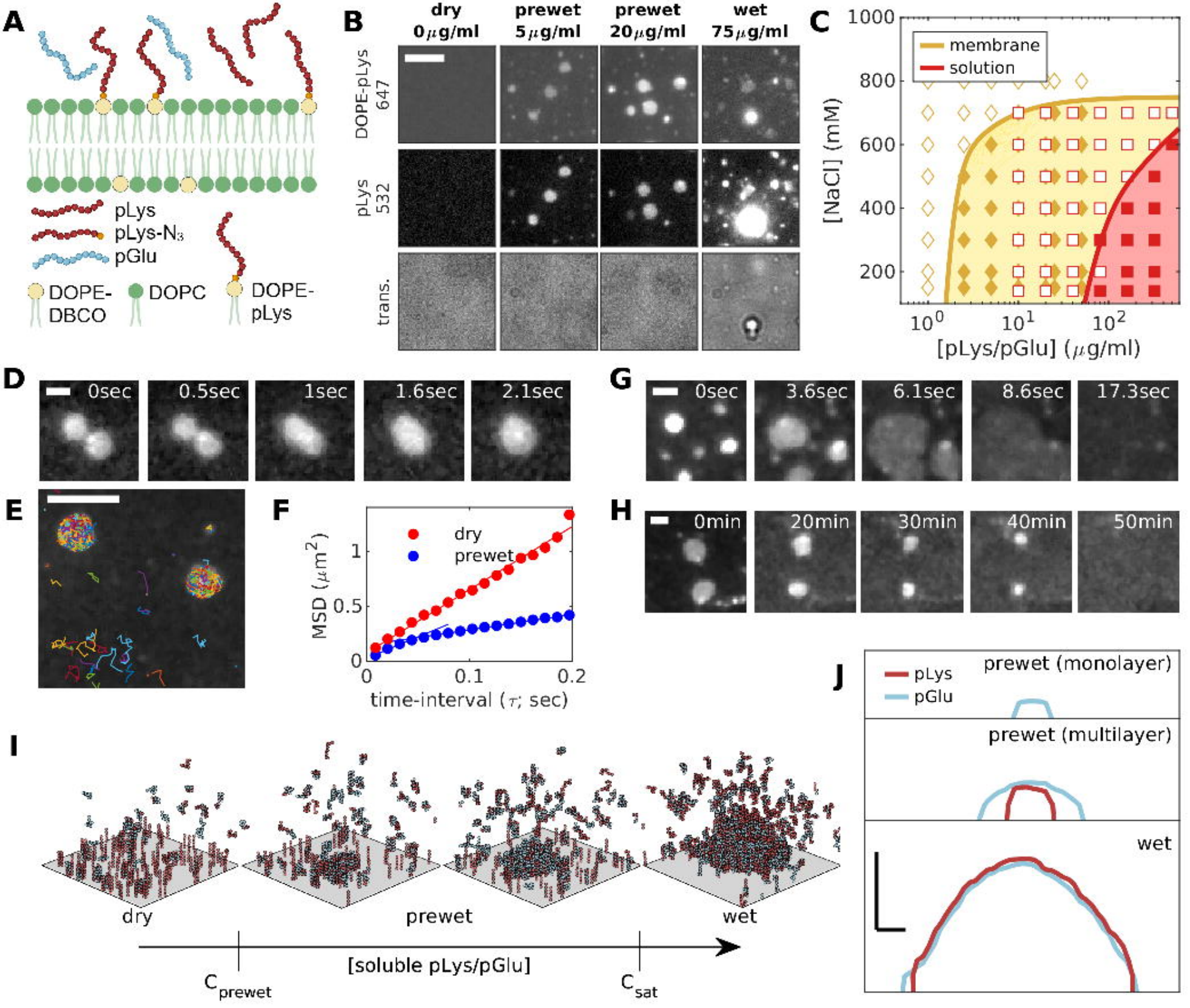
A
pLys
pLys-N3
pGlu
DOPE-DBCO
DOPC
DOPE-pLys
B
dry 0μg/ml
prewet 5μg/ml
prewet 20μg/ml
wet 75μg/ml
DOPE-pLys 647
pLys 532
trans.
C
membrane
solution
[NaCl] (mM)
[pLys/pGlu] (μg/ml)
D
0sec
0.5sec
1sec
1.6sec
2.1sec
E
F
dry
prewet
MSD (μm²)
time-interval (τ; sec)
G
0sec
3.6sec
6.1sec
8.6sec
17.3sec
H
0min
20min
30min
40min
50min
I
dry
prewet
wet
[soluble pLys/pGlu]
C prewet
C sat
J
pLys
pGlu
prewet (monolayer)
prewet (multilayer)
wet

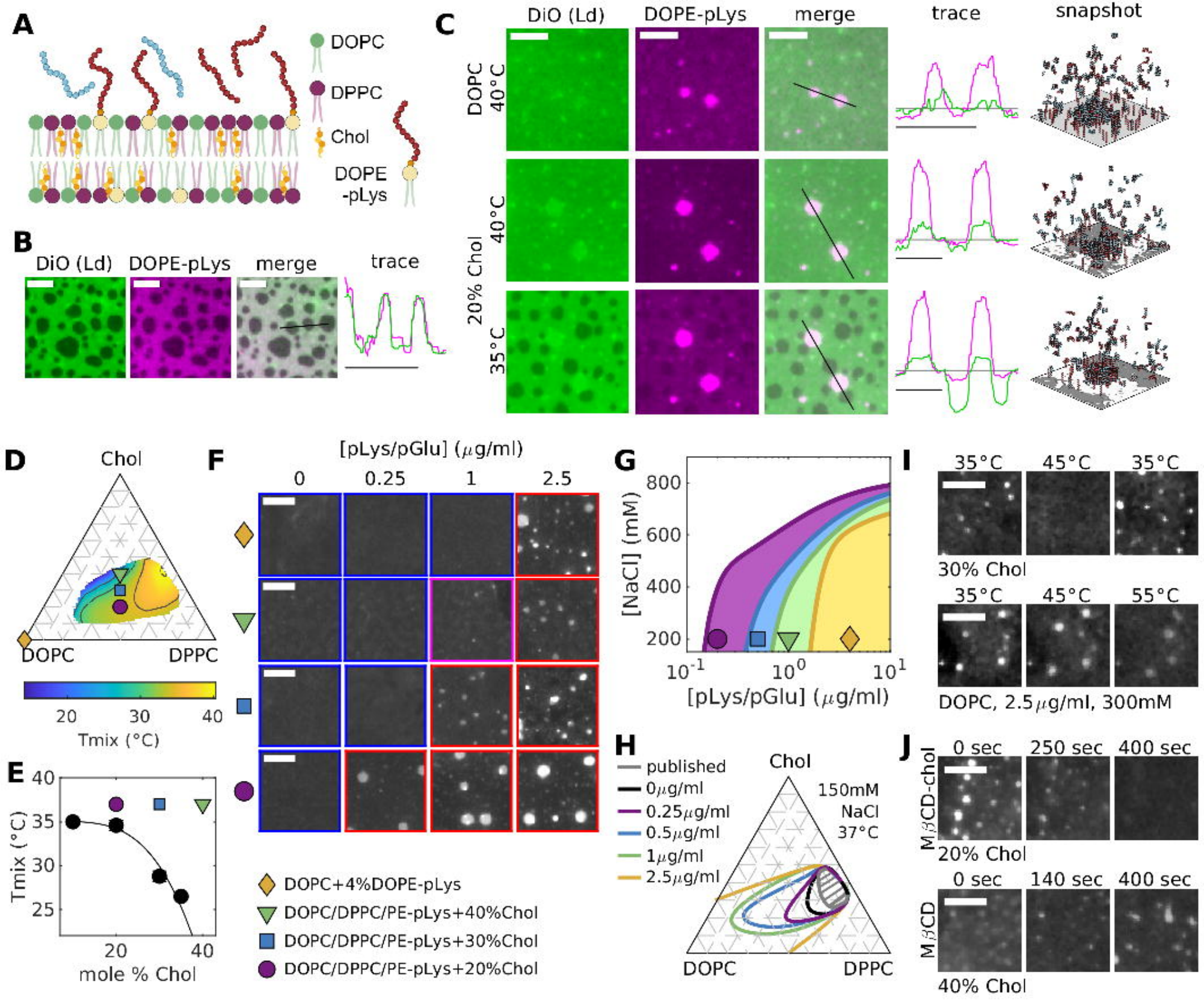
A
DOPC
DPPC
Chol
DOPE
-pLys
B
DiO (Ld)
DOPE-pLys
merge
trace
C
DiO (Ld)
DOPE-pLys
merge
trace
snapshot
DOPC
40°C
40°C
20% Chol
35°C
D
Chol
DOPC
DPPC
20
30
40
Tmix (°C)
E
Tmix (°C)
mole % Chol
F
[pLys/pGlu] (μg/ml)
0
0.25
1
2.5
DOPC+4%DOPE-pLys
DOPC/DPPC/PE-pLys+40%Chol
DOPC/DPPC/PE-pLys+30%Chol
DOPC/DPPC/PE-pLys+20%Chol
G
[NaCl] (mM)
[pLys/pGlu] (μg/ml)
H
published
0μg/ml
0.25μg/ml
0.5μg/ml
1μg/ml
2.5μg/ml
Chol
150mM
NaCl
37°C
DOPC
DPPC
I
35°C
45°C
35°C
30% Chol
35°C
45°C
55°C
DOPC, 2.5μg/ml, 300mM
J
0 sec
250 sec
400 sec
MβCD-chol
20% Chol
0 sec
140 sec
400 sec
MβCD
40% Chol

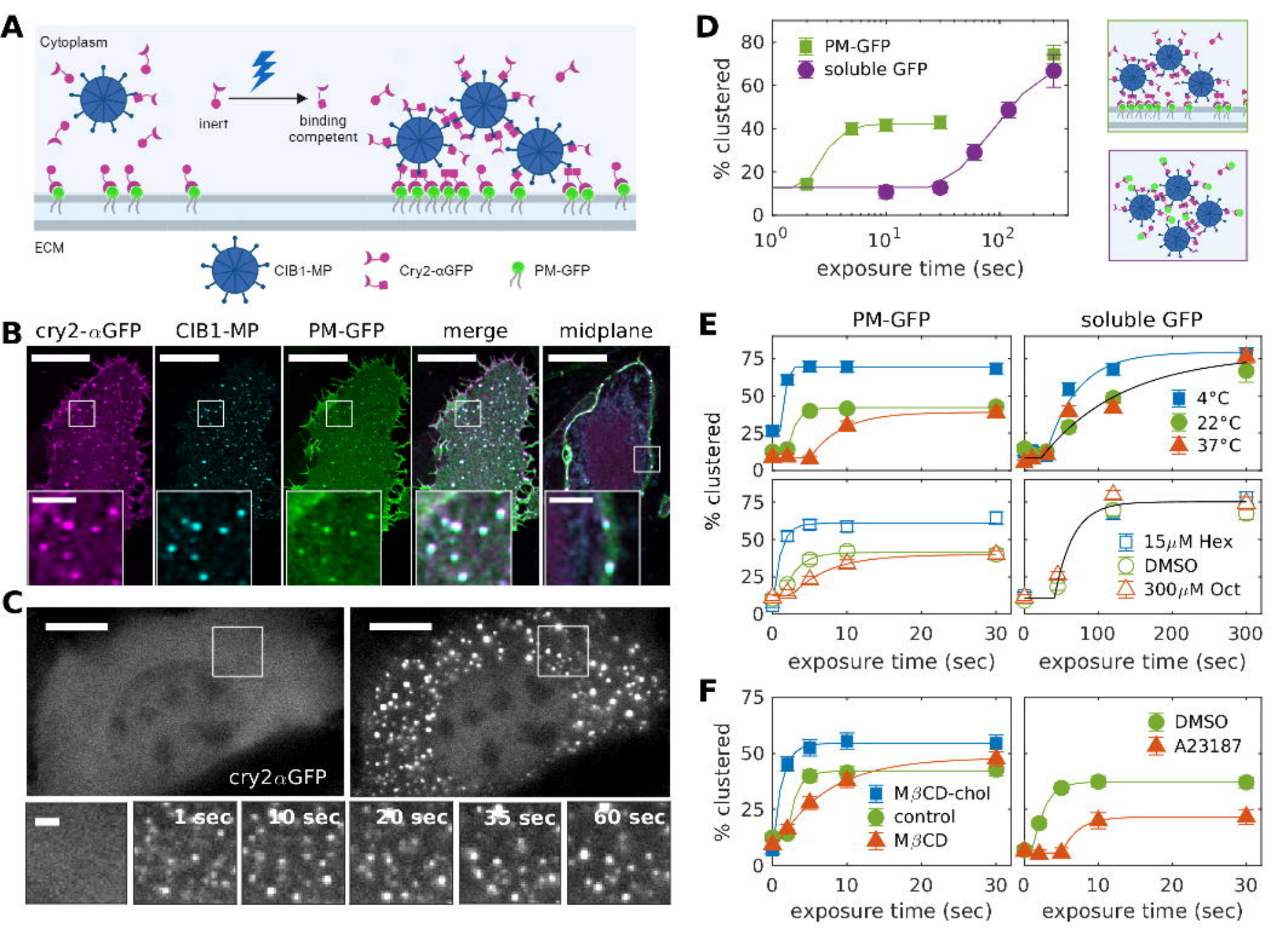
A
Cytoplasm
inert
binding competent
ECM
CIB1-MP
Cry2-αGFP
PM-GFP
B
cry2-αGFP
CIB1-MP
PM-GFP
merge
midplane
C
cry2αGFP
1 sec
10 sec
20 sec
35 sec
60 sec
D
PM-GFP
soluble GFP
% clustered
exposure time (sec)
E
PM-GFP
soluble GFP
% clustered
4°C
22°C
37°C
15μM Hex
DMSO
300μM Oct
exposure time (sec)
F
% clustered
MβCD-chol
control
MβCD
DMSO
A23187
exposure time (sec)